# Synthesis and Structural-Bonding Analysis of $(\eta^5\text{-}C_5H_4Me)_4Fe_4(CO)_6P_8$ and $(\eta^5\text{-}C_5H_4Me)_4Fe_6(CO)_{13}P_8$: Two Unprecedented Transition-Metal Complexes Containing the Cage-like $P_8$ Subunit of Hittorf's Monoclinic Phosphorus Allotrope

**Mary E. Barr,[1a] Bruce R. Adams,[1a] Robert R. Weller,[1b,c] and Lawrence F. Dahl*,[1a]**

*Contribution from the Department of Chemistry, University of Wisconsin—Madison, 1101 University Avenue, Madison, Wisconsin 53706, and EXTREL FTMS, 6416 Schroeder Road, Madison, Wisconsin 53711.* *Received October 3, 1990*

**Abstract:** As part of our investigation into the photochemical reactions of $P_4$ with transition-metal carbonyl and organometallic precursors, we generated $Cp'_4Fe_4(CO)_6P_8$ (**1**) (where Cp' denotes $\eta^5\text{-}C_5H_4Me$) (11% yield) by cophotolysis of $[Cp'Fe(CO)_2]_2$ and $P_4$. In addition, we have synthesized $Cp'_4Fe_6(CO)_{13}P_8$ (**2**) (40–50% yield) via a nonphotolytic reaction of **1** with sources of the electron-deficient $Fe(CO)_4$ fragment. Both compounds were characterized by single-crystal X-ray diffraction, laser desorption FT mass spectrometry, and spectroscopic ($^1H$, $^{31}P$ NMR; IR) and electrochemical measurements. **1** and **2** are the first examples of transition-metal polyphosphide complexes containing a realgar-type $\alpha\text{-}P_8$ core. This $P_8$ cage, with four nonbonding planar phosphorus atoms coordinated to two bonding pairs of tetrahedrally related bridgehead phosphorus atoms above and below the plane, is one component of Hittorf's elemental phosphorus (**3**). While **3** has a complicated tube-like cross-linked polymeric structure consisting of alternating $P_8$ and $P_9$ cage subunits linked by $\mu_2\text{-}P_2$ bridges, the molecular compounds **1** and **2** each contain a $P_8$ cage with two $\mu_2\text{-}FeCp'(CO)$ single-atom bridging ligands which chelate two opposite pairs of the planar phosphorus atoms. Two additional nonbridging $FeCp'(CO)_2$ substituents in **1** are coordinated to two diagonally related planar phosphorus atoms, resulting in a pseudo-$C_2$ molecular geometry. Formation of **2** from **1** involves the coordination of two Lewis acid $Fe(CO)_4$ adducts to the other two planar phosphorus atoms, followed by loss of a CO from one adduct and concomitant electron-pair Fe–Fe bonding with the adjacent terminal $FeCp'(CO)_2$ group. The $\alpha\text{-}P_8$ cages of **1** and **2** are primarily stabilized by two $\mu_2$-Fe chelating atoms; evidence of this $\alpha\text{-}P_8$ cage stabilization is given by LD/FTMS data in which all $P_8$-containing ion fragments invariably include at least two FeCp' groups. An indication of additional stabilization by the electron-deficient iron substituents in **1** and **2** is derived from a comparative analysis of geometrical differences in their $P_8$ cages with those in Hittorf's violet phosphorus (**3**) and $P_8(P_2iPr_2)_2$ (**4**) (where iPr denotes isopropyl) and with the electronically equivalent $\alpha\text{-}P_4S_4$ molecule (**5**); the significantly shorter bridgehead P–P single-bond distances in **1** and **2**, relative to those in **3**, **4**, and **5**, are presumed to be a consequence of markedly reduced repulsions between the nonbonding electron pairs on these bridgehead phosphorus atoms. Crystal data for $(\eta^5\text{-}C_5H_4CH_3)_4Fe_4(CO)_6P_8$, **1** are as follows: fw = 955.73 g/mol; monoclinic, $P2_1/c$; $a$ = 15.305 (6) Å, $b$ = 9.650 (2) Å, $c$ = 24.532 (4) Å, $\beta$ = 97.71 (2)°, $V$ = 3590 (2) Å$^3$ at −100 °C; $d_{(calcd)}$ = 1.74 g/cm$^3$ for $Z$ = 4; least-squares refinement converged at $R_1(F)$ = 0.040, $R_2(F)$ = 0.052. Crystal data for $(\eta^5\text{-}C_5H_4CH_3)_4Fe_6(CO)_{13}P_8$, **2**, are as follows: fw = 1263.49 g/mol; monoclinic, $P2_1/c$; $a$ = 7.587 (2) Å, $b$ = 27.073 (8) Å, $c$ = 22.021 (7) Å, $\beta$ = 99.12 (2)°, $V$ = 4466 (2) Å$^3$ at −100 °C; $d_{(calcd)}$ = 1.88 g/cm$^3$ for $Z$ = 4; $R_1(F)$ = 0.066, $R_2(F)$ = 0.071.

## Introduction

During this past decade, phosphorus chemistry has undergone a remarkable renaissance, due in part to its integration with transition-metal chemistry. A number of excellent reviews[2-11] have examined various aspects of the intriguing diversity of new polyphosphide and metal–phosphorus complexes. Studies first reported in 1984 by Scherer and co-workers[12] on the syntheses and structures of compounds in which cyclic phosphido ligands are coordinated to cyclopentadienyl metal fragments revived our previous interest in metal carbonyl and cyclopentadienyl phosphide and arsenide clusters.[13]

Typically, thermolytic reactions between cyclopentadienyl metal carbonyl complexes and $P_4$ are carried out in relatively high-boiling solvents such as toluene or xylene.[12] Such vigorous procedures often give rise to insoluble residues with resulting low yields of the desired compounds, due in part to the number of different complexes formed. Furthermore, the variety of synthetic methods which yield bare phosphido systems, from reagents as diverse as $PCl_3$,[14] $P_4S_3$,[15] and $P_4$,[12,13b,16] suggests that there are no unambiguous mechanisms for their formation. Thus, a gentle, nonthermolytic procedure that would activate both $P_4$ and the organometallic reagent was deemed desirable in order to improve yields as well as to isolate novel metal phosphide systems which are thermally sensitive.

We hypothesized that a reasonable alternative to a thermal synthetic method would be a photochemical one. While solid $P_4$ requires strenuous thermal conditions for dissociation into $P_2$ fragments,[17] $P_4$ in solution photolyzes readily to $P_2$ at ambient

(1) (a) University of Wisconsin—Madison. (b) EXTREL FTMS. (c) Present address: Westinghouse Savannah River Company, P.O. Box 616, Bldg 735A, Aiken, SC 29802.

(2) (a) Scherer, O. J. *Angew. Chem., Int. Ed. Engl.* **1985**, *24*, 924. (b) Scherer, O. J. *Comments Inorg. Chem.* **1987**, *6*, 1.

(3) Baudler, M. *Angew. Chem., Int. Ed. Engl.* **1987**, *26*, 419.

(4) (a) von Schnering, H.-G. *Angew. Chem., Int. Ed. Engl.* **1981**, *20*, 33. (b) von Schnering, H.-G.; Hönle, W. *Chem. Rev.* **1988**, *88*, 243.

(5) Di Vaira, M.; Stoppioni, P.; Peruzzini, M. *Polyhedron* **1987**, *6*, 351.

(6) Dimaio, A.-J.; Rheingold, A. L. *Chem. Rev.* **1990**, *90*, 169.

(7) Veith, M. *Chem. Rev.* **1990**, *90*, 3.

(8) Fenske, D.; Ohmer, J.; Hachgenei, J.; Merzweiler, K. *Angew. Chem., Int. Ed. Engl.* **1988**, *27*, 1277.

(9) Whitmire, K. H. *J. Coord. Chem.* **1988**, *17*, 95.

(10) Huttner, G.; Knoll, K. *Angew. Chem., Int. Ed. Engl.* **1987**, *26*, 743.

(11) (a) Cowley, A. H. *Phosphorus Sulfur* **1987**, *30*, 129. (b) Cowley, A. H. *Phosphorus Sulfur* **1986**, *26*, 31. (c) Arif, A. M.; Jones, R. A.; Schwab, S. T. *J. Coord. Chem.* **1987**, *16*, 51. (d) Jones, R. A.; Stuart, A. L.; Atwood, J. L.; Hunter, W. E. *Organometallics* **1983**, *2*, 874.

(12) (a) Scherer, O. J.; Sitzmann, H.; Wolmershäuser, G. *J. Organomet. Chem.* **1984**, *268*, C9. (b) Scherer, O. J.; Sitzmann, H.; Wolmershäuser, G. *Angew. Chem., Int. Ed. Engl.* **1985**, *24*, 351. (c) Scherer, O. J.; Schwalb, J.; Wolmershäuser, G.; Kaim, W.; Gross, R. *Angew. Chem., Int. Ed. Engl.* **1986**, *25*, 363. (d) Scherer, O. J.; Brück, T. *Angew. Chem., Int. Ed. Engl.* **1987**, *26*, 59.

(13) (a) Foust, A.; Foster, M. S.; Dahl, L. F. *J. Am. Chem. Soc.* **1969**, *91*, 5631. (b) Simon, G. L.; Dahl, L. F. *J. Am. Chem. Soc.* **1973**, *95*, 2175. (c) Campana, C. E.; Vizi-Orosz, A.; Pályi, G.; Markó, L.; Dahl, L. F. *Inorg. Chem.* **1979**, *18*, 3054.

(14) Vizi-Orosz, A.; Pályi, G.; Markó, L. *J. Organomet. Chem.* **1973**, *60*, C25.

(15) DiVaira, M.; Sacconi, L.; Stoppioni, P. *J. Organomet. Chem.* **1983**, *250*, 183.

(16) (a) Goh, L. Y.; Wong, R. C. S.; Chu, C. K. *J. Chem. Soc., Dalton Trans.* **1990**, 997. (b) Ghilardi, C. A.; Midollini, S.; Orlandini, A.; Sacconi, L. *Inorg. Chem.* **1980**, *19*, 301.

(17) Melville, H. W.; Gray, S. C. *Trans. Faraday Soc.* **1936**, *32*, 271.

0002-7863/91/1513-3052$02.50/0 

temperatures.[18] Thus, photolysis of $P_4$ in situ with solutions containing organometallic precursors would generally be preferable to thermolysis for a number of reasons: (1) room- or low-temperature photolysis would reduce decomposition of thermally unstable intermediates or products; (2) the reactions could be performed in a wider variety of solvents (polar and nonpolar, coordinating and noncoordinating) determined only by the solubilities of the reactants, instead of the necessarily high-reflux temperatures; and (3) varying the photolytic wavelength could influence the formation of even- versus odd-membered phosphido systems, since $P_4$ dissociates to $P_2$ in low-energy ultraviolet light, while $P_2$ dissociates to P atoms under mid-energy ultraviolet light.[19] Although only a few of these parameters have been varied for any given system, syntheses in our laboratories of the 34-electron $Cp^*_2Fe_2(\mu_2\text{-}P_2)_2$ and 36-electron $Cp^*_2Co_2(\mu_2\text{-}P_2)_2$ dimers[20a] (where $Cp^*$ denotes $\eta^5\text{-}C_5Me_5$) and other polyphosphido complexes[21] in addition to the title compound **1** have substantiated the utility of this photolytic synthetic method. During the period in which this work was in progress, Scherer and co-workers[22] reported the syntheses and characterizations of $Cp^*Nb(CO)_2P_4$ and its arsenido analogue under approximately similar photolytic reaction conditions.

$Cp'_4Fe_4(CO)_6P_8$ (**1**), generated via a currently underutilized photosynthetic method, and its derivative $Cp'_4Fe_6(CO)_{13}P_8$ (**2**), presented herein, represent a new class of transition-metal polyphosphide cage structures which has not been previously generated by using traditional thermolytic procedures. The polyphosphide $P_8$ cages in **1** and **2** exhibit thermal stabilities that are unusual for such an architecture; the existence of **1** and **2** is attributed primarily to the stabilizing effects of their two chelating iron groups as well as to the electron-deficient nature of the cage substituents.

## Experimental Section

**General Procedures.** All reactions, sample transfers, and manipulations were performed with oven-dried standard Schlenk-type glassware under nitrogen, either on a vacuum line, in a glovebag, or in a Vacuum Atmospheres glovebox. The following solvents were dried and distilled prior to use: THF (potassium), $CH_2Cl_2$ ($CaH_2$), toluene (sodium), diisopropyl ether (potassium), and hexane (Skelly B cut, $CaH_2$). $Fe_2(CO)_9$ was prepared via a well-established procedure,[23] and $[Cp'Fe(CO)_2]_2$ was prepared via a minor modification of the standard preparation[24] for $[CpFe(CO)_2]_2$. $Me_3NO\cdot 2H_2O$ (Aldrich) was dried and sublimed prior to use. $P_4$ (Strem) and $Fe(CO)_5$ (Aldrich) were used without further purification.

Solution and solid-state infrared spectra were recorded on a Beckman 4240 spectrophotometer. NMR spectra were obtained with a Varian VXR-500 spectrometer. Cyclic voltammograms were obtained with a BAS-100 Electrochemical Analyzer with the electrochemical cell enclosed in a nitrogen-filled Vacuum Atmospheres glovebox. Electrochemical measurements were carried out in $CH_2Cl_2$, THF, or $CH_3CN$ containing 0.1 M $[NBu_4][PF_6]$. The working electrode was a platinum disk, and the reference electrode was a Vycor-tipped aqueous SCE separated from the test solution by a Vycor-tipped salt bridge filled with a 0.1 M $[NBu_4][PF_6]/CH_3CN$ solution. The auxiliary electrode was a platinum coil. Each test solution consisted of ca. 7 mL of solvent containing approximately $10^{-3}$ M compound.

Mass spectra were obtained with an EXTREL FTMS-2000 Fourier transform (FT) mass spectrometer equipped with a 3.0-T superconducting magnet, an EXTREL laser desorption (LD) interface, and a Tachisto 215G pulsed infrared $CO_2$ laser operated as an aperature-controlled stable resonator. Additional details of the LD-FTMS instrument and procedures for data collection are available elsewhere.[20]

**Preparation and Physical Properties of $Cp'_4Fe_4(CO)_6P_8$ (1).** In a typical reaction, $[Cp'Fe(CO)_2]_2$ (0.36 g, 0.94 mmol) and an equimolar amount of $P_4$ (0.12 g, 0.96 mmol) were dissolved in ~200 mL of toluene and transferred to a water-cooled Pyrex photolysis apparatus. The mixture was irradiated at room temperature for approximately 2 h with a Hanovia 450 W medium-pressure Hg vapor lamp until IR spectra indicated that most of the starting dimer was consumed. The solution color changed from red to red-brown during the course of the photolysis. The solvent was removed overnight under a nitrogen purge. The resulting solid was extracted (3×) with a 50/50 (v/v) hexane/toluene mixture and chromatographed on a 2.5 (width) × 15 (length) cm silica gel column (Bio-sil A, 200–325 mesh) packed with the same solvent mixture. Colorless $P_4$ was eluted with the solvent front. A small amount of unreacted $[Cp'Fe(CO)_2]_2$ and the orange-red **1** (0.05 g, 11% yield) were eluted with toluene. After **1** was eluted, a substantial amount of material remained strongly adsorbed to the silica gel. The small amount of adsorbed material which could be eluted with THF displayed an IR spectrum similar to the solid remaining from the original hexane/toluene extractions. This dark brown material is the major product and is not yet fully characterized.

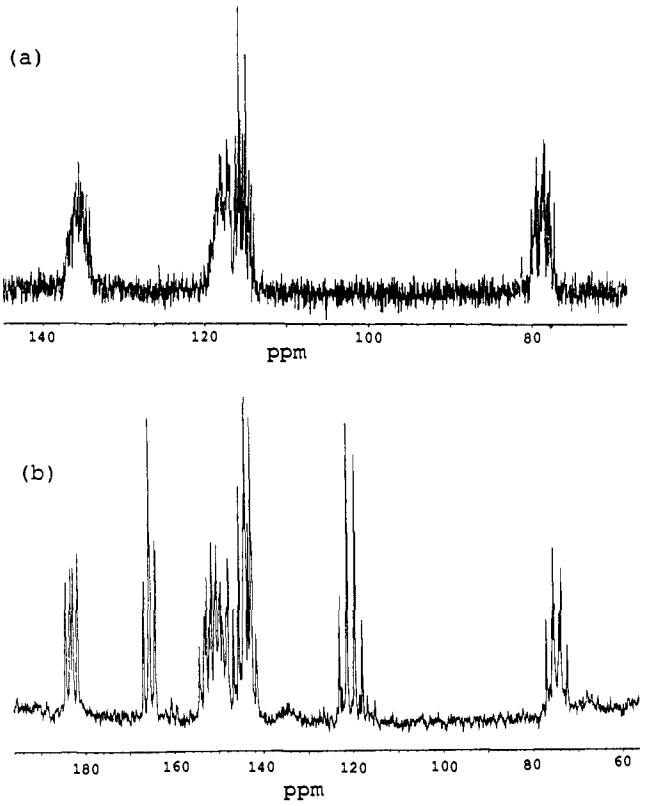


**Figure 1.** $^{31}P\{^1H\}$ NMR spectra for (a) $Cp'_4Fe_4(CO)_6P_8$ (**1**) and (b) $Cp'_4Fe_6(CO)_{13}P_8$ (**2**).

A low-temperature photolysis in a dry ice/ethanol bath gave a distribution of products similar to those of the room-temperature reactions. Solutions of **1** are quite air-sensitive, but the solid does not decompose when it is briefly exposed to air.

An infrared spectrum of **1** in THF exhibits three carbonyl peaks of similar intensities at 2010 (s), 1975 (s), and 1920 (s) $cm^{-1}$. A solid-state spectrum (KBr) shows absorption bands at 2005, 1965, and 1895 $cm^{-1}$. A $^1H$ NMR spectrum (499.8 MHz, $CDCl_3$, TMS internal) of **1** contains only resonances due to the four methylcyclopentadienyl ligands at $\delta$ 1.81 (s, 3 H) and 2.00 (br s, 9 H) ppm for the 12 methyl protons and eight peaks (~2 H each) in the range of $\delta$ 4–5 ppm corresponding to the 16 ring protons. A $^{31}P\{^1H\}$ NMR spectrum (202.3 MHz, $CDCl_3$, 85% $H_3PO_4$ external) exhibits four complex second-order resonances of approximately equal intensities centered at $\delta$ 82, 119, 121, and 138 ppm (Figure 1a).

Both positive- and negative-ion LD/FT mass spectra of **1** (Figure 2) contain many high-mass ion signals consistent with its stoichiometry and architecture. The fragment-ion pattern observed in the positive-ion LD/FT mass spectrum includes the parent ion peak at $m/z$ 956 ($[M]^+$, 31%) as well as other $P_8$-containing ion peaks at $m/z$ 928 ($[M - CO]^+$, 42%), 900 ($[M - 2\,CO]^+$, 12%), and 737 ($[Cp'_3Fe_3(CO)_3P_8]^+$, 100%). The negative-ion mass spectrum also displays a number of $P_8$-containing ion fragments at $m/z$ 765 ($[Cp'_3Fe_3(CO)_4P_8]^-$, 27%), 737 ($[Cp'_3Fe_3(CO)_3P_8]^-$, 10%), 709 ($[Cp'_3Fe_3(CO)_2P_8]^-$, 94%), 546 ($[Cp'_2Fe_2(CO)P_8]^-$, 100%), and 518 ($[Cp'_2Fe_2P_8]^-$, 11%).

**Preparation and Physical Properties of $Cp'_4Fe_6(CO)_{13}P_8$ (2) from $Cp'_4Fe_4(CO)_6P_8$ (1). (a) First Method.** A solution of **1** (0.2 g, 0.2 mmol)

(18) Rathenqu, G. *Physica* **1937**, *4*, 503.
(19) Gaydon, A. G. *Dissociation Energies and Spectra of Diatomic Molecules*, 3rd ed.; Chapman and Hall: London, 1968; p 279.
(20) (a) Bjarnason, A.; DesEnfants, II, R. E.; Barr, M. E.; Dahl, L. F. *Organometallics* **1990**, *9*, 657. (b) Bjarnason, A. *Rapid Commun. Mass Spectrom.* **1989**, *3*, 373.
(21) Barr, M. E.; Dahl, L. F. Unpublished results.
(22) (a) Scherer, O. J.; Vondung, J.; Wolmershäuser, G. *Angew. Chem., Int. Ed. Engl.* **1989**, *28*, 1355. (b) Scherer, O. J.; Vondung, J.; Wolmershäuser, G. *J. Organomet. Chem.* **1989**, *376*, C35.

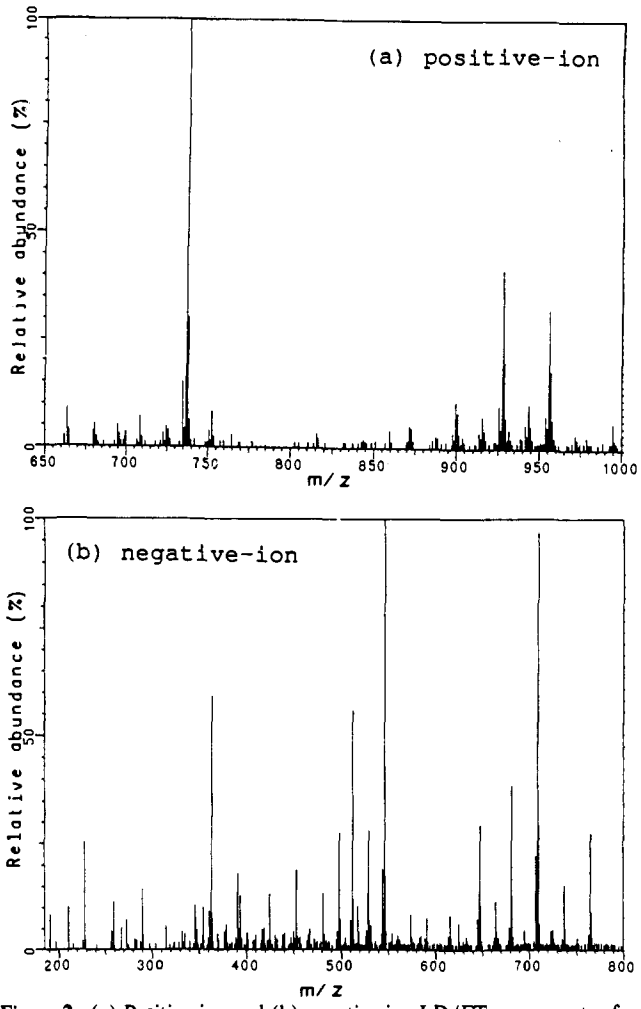


**Figure 2.** (a) Positive-ion and (b) negative-ion LD/FT mass spectra for $Cp'_4Fe_4(CO)_6P_8$ (**1**).

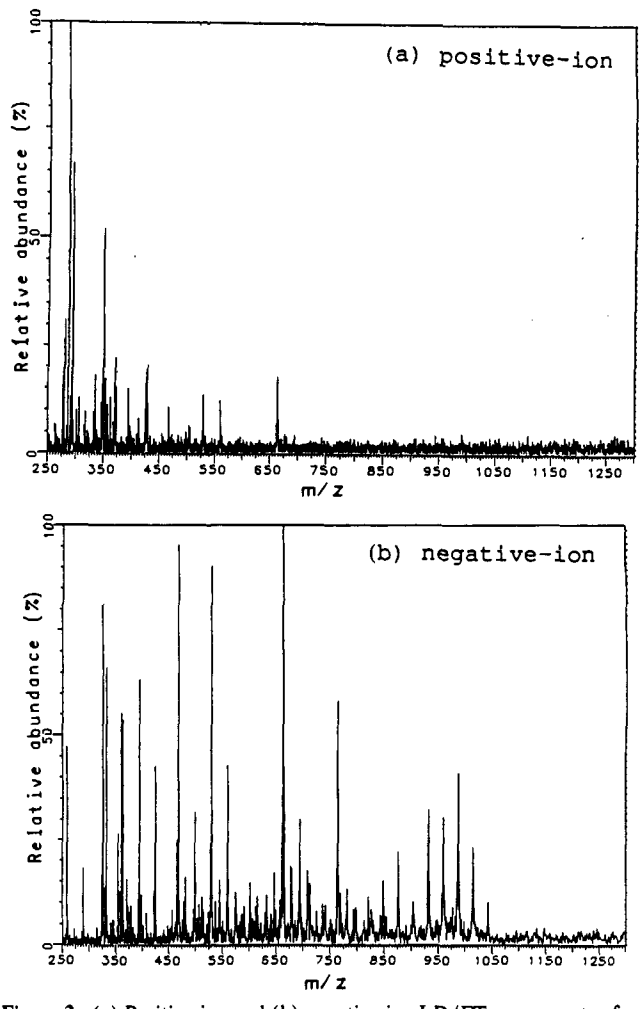


**Figure 3.** (a) Positive-ion and (b) negative-ion LD/FT mass spectra for $Cp'_4Fe_6(CO)_{13}P_8$ (**2**).

in 50 mL of THF was added to a slurry of $Fe(CO)_5$ (0.15 mL, 1.1 mmol) and $Me_3NO$ (0.07 g, 0.9 mmol) in 10 mL of THF and stirred for 2 h. The solution changed from the orange color of **1** to a deep green within 1 h. Solvent and excess $Fe(CO)_5$ were then removed under vacuum. The resulting solid material was extracted (2×) with toluene. The toluene extract was reduced to approximately 1 mL and loaded onto a 0.8 (width) × 10 (length) cm silica gel column (Bio-sil A) packed in toluene. Compound **2**, $Cp'_4Fe_6(CO)_{13}P_8$ (0.11 g, ~40% yield), was eluted as an olive green band with toluene.

**(b) Second Method.** **1** (0.1 g, 0.1 mmol) and $Fe_2(CO)_9$ (0.2 g, 0.5 mmol) were slurried in 50 mL of THF overnight at room temperature. After the solvent was removed under vacuum, the resulting dark solid was extracted with toluene, leaving behind some unreacted $Fe_2(CO)_9$ and a trace of black residue. The toluene extract was chromatographed, as in the first method, to give **2** (0.06 g, ~50% yield). **2** is only moderately air-sensitive as a solid but decomposes quickly when exposed to air in solution.

A solid-state infrared spectrum (KBr) of **2** exhibits carbonyl absorption bands at 2040 (m, sh), 2020 (m), 1980 (s), 1965 (sh), 1950 (sh), 1930 (s), 1895 (m), and 1755 (m) $cm^{-1}$. A $^1H$ NMR spectrum (499.8 MHz, $CDCl_3$, TMS internal) of **2** shows methyl hydrogen resonances for the four methylcyclopentadienyl ligands at $\delta$ 1.93, 2.00, 2.03, and 2.07 ppm (s, 3 H each) and a set of 16 peaks (s, 16 H) for the ring hydrogens in the region of $\delta$ 4.05–5.30 ppm. A $^{31}P\{^1H\}$ NMR spectrum (202.3 MHz, $CDCl_3$, 85% $H_3PO_4$ external) displays resonances at $\delta$ 75 (d/t, $J_{(P-P)}$ = 343/294 Hz, 1 P), 123 (q, $J_{(P-P)}$ = 343 Hz, 1 P), 147 (m, 2 P), 154 (m, 2 P), 169 (t/d, $J_{(P-P)}$ = 283/27 Hz, 1 P), and 186 (d/d, $J_{(P-P)}$ = 340/119 Hz, 1 P) ppm (Figure 1b).

A negative-ion LD/FT mass spectrum of **2** (Figure 3b) displays a number of structurally consistent high-mass ion peaks. Signals assigned to $P_8$-containing ion fragments include $m/z$ 1045 ($[Cp'_3Fe_5(CO)_{10}P_8]^-$, 10%), 989 ($[Cp'_3Fe_5(CO)_8P_8]^-$, 41%), 765 ($[Cp'_3Fe_4(CO)_2P_8]^-$, 58%), 709 ($[Cp'_3Fe_4P_8]^-$, 18%), and a number of other relatively abundant (10–40%) ion peaks which occur at 28 amu intervals between $m/z$ 1017 and 821. The most abundant negative-ion peak is at $m/z$ 664 ($[Cp'_4Fe_4P_4]^-$, 100%); a positive-ion mass spectrum of **2** (Figure 3a) contains only this ion fragment and lower mass ion peaks.

**X-ray Crystallographic Determinations of $Cp'_4Fe_4(CO)_6P_8$ (1) and $Cp'_4Fe_6(CO)_{13}P_8$ (2). (a) General Procedures.** Intensity data for the two compounds were collected with graphite-monochromated Mo K$\alpha$ radiation on a Siemens (Nicolet) P3F diffractometer equipped with a liquid-nitrogen cooling apparatus. The procedures involved in crystal alignment and data collection are described elsewhere.[25] Crystal data, data-collection parameters, and least-squares refinement parameters for each structure are presented in Table I. Cell dimensions and their esd's were obtained from a least-squares analysis of 20 well-centered, high-angle reflections (ca. 18–23° in 2$\theta$). The intensities of three chosen standard reflections for **1** and **2** did not vary significantly (<3%) during the data collections. Atomic scattering factors for neutral atoms were used together with anomalous dispersion corrections for all non-hydrogen atoms. Hydrogen atoms were inserted at idealized positions with fixed isotropic thermal parameters and were included in the final stages of refinement.

**(b) $Cp'_4Fe_4(CO)_6P_8$ (1).** Crystals suitable for X-ray analysis were grown by a slow, layered diffusion of hexane into a concentrated THF solution of the compound. A red-orange parallelepiped-shaped crystal of approximate dimensions 0.3 × 0.6 × 0.4 mm was mounted on a glass fiber, affixed with epoxy, and coated with paratone-N to exclude air. Axial photographs verified the lattice lengths and symmetry of the chosen monoclinic unit cell. Systematic absences of $0k0$ for $k$ odd and $h0l$ for $l$ odd indicated the space group to be $P2_1/c$ ($C_{2h}$, no. 14). Direct methods (SHELXTL PLUS 4.11)[26] were used to locate the eight phosphorus and four iron atoms comprising one crystallographically independent molecule. The other non-hydrogen atoms were located from difference Fourier

(23) Braye, E. H.; Hübel, W. *Inorg. Synth.* **1966**, *8*, 178.
(24) King, R. B. *Organometallic Synth.*; Academic: New York, 1965, Vol. 1.
(25) Byers, L. R.; Dahl, L. F. *Inorg. Chem.* **1980**, *19*, 277.
(26) SHELXTL PLUS 4.11, Siemens Analytical X-ray Instruments, Inc., 600 Enterprise Lane, Madison, WI 53719-1173.

**Table I.** Crystal, Data Collection, and Structural Refinement Parameters for $Cp'_4Fe_4(CO)_6P_8$ (**1**) and $Cp'_4Fe_6(CO)_{13}P_8$ (**2**)

| | **1** | **2** |
|---|---|---|
| fw, g/mol | 955.73 | 1263.49 |
| cryst system | monoclinic | monoclinic |
| cell const temp, °C | −100 | −100 |
| $a$, Å | 15.305 (6) | 7.587 (2) |
| $b$, Å | 9.650 (2) | 27.073 (8) |
| $c$, Å | 24.532 (4) | 22.021 (7) |
| $\alpha$, $\beta$, $\gamma$, deg | 90, 97.71 (2), 90 | 90, 99.12 (2), 90 |
| $V$, Å$^3$ | 3590 (2) | 4466 (2) |
| space group | $P2_1/c$ | $P2_1/c$ |
| $Z$ | 4 | 4 |
| $d_{calcd}$, g/cm$^3$ | 1.743 | 1.879 |
| $\mu$, cm$^{-1}$ | 19.5 | 22.4 |
| data collection temp, °C | −100 | −100 |
| radiation | Mo K$\alpha$ | Mo K$\alpha$ |
| scan mode | Wyckoff | Wyckoff |
| scan speed, deg/min | variable (2–15) | variable (2–20) |
| scan range, deg | 0.4 | 0.5 |
| background offset, deg | 0.6 | 0.4 |
| $2\theta$ limits, deg | 3–50 | 3–47 |
| no. of data collected | 7027 | 7260 |
| cutoff for obsd data | $\|F\| < 4\sigma(F)$ | $\|F\| < 4\sigma(F)$ |
| no. of ind obsd data | 4742 | 4093 |
| data/parameter | 11.0/1 | 7.2/1 |
| wght | 0.0015 (refined) | 0.0009 (fixed) |
| $R_1(F)$, $R_2(F)$, % | 3.99, 5.23 | 6.58, 7.08 |
| goodness-of-fit, GOF | 1.05 | 1.43 |

syntheses coupled with least-squares refinement (SHELXTL PLUS 4.11).[26] An empirical $\psi$-scan absorption correction was applied to the intensity data. All non-hydrogen atoms were refined anisotropically. The final difference Fourier map, which displayed a maximum residual electron density of 0.5 e$^-$/Å$^3$, did not reveal any unusual features.

Selected interatomic distances and bond angles are presented in Table II. Tables of coordinates for all non-hydrogen atoms of **1**, coordinates for the hydrogen atoms, anisotropic thermal parameters for all non-hydrogen atoms, and observed and calculated structure factor amplitudes are available as supplementary material.

**(c) $Cp'_4Fe_6(CO)_{13}P_8$ (2).** Crystals were grown by a slow, layered diffusion of diisopropyl ether into a concentrated THF solution containing the compound. A dark green needle of dimensions 0.10 × 0.08 × 0.55 mm was mounted on a glass fiber parallel to the long axis, affixed with epoxy, and coated with paratone-N. Axial photographs substantiated the dimensions and symmetry of the chosen monoclinic unit cell. Systematic absences indicated the probable space group to be $P2_1/c$ ($C_{2h}$, no. 14). Direct methods (SHELXTL PLUS 4.11)[26] were used to locate the eight phosphorus and six iron atoms of the crystallographically independent molecule. The other non-hydrogen atoms were located from difference Fourier syntheses coupled with least-squares refinement (SHELXTL PLUS 4.11).[26] An empirical $\psi$-scan absorption correction was applied to the intensity data. Since the thermal parameters for one of the carbonyl carbon atoms, C(11), persisted in going nonpositive definite when refined anisotropically, its temperature factor was kept isotropic. All other non-hydrogen atoms were refined anisotropically. The final difference map with a maximum residual electron density of 1.1 e$^-$/Å$^3$ gave no indication of crystal disorder nor the presence of any solvent molecules.

Selected interatomic distances and bond angles are presented in Table III. Tables of coordinates for the non-hydrogen atoms of **2**, coordinates for the hydrogen atoms, anisotropic thermal parameters for all non-hydrogen atoms, and observed and calculated structure factor amplitudes are available as supplementary material.

## Results and Discussion

**Crystal and Molecular Structural Features of $Cp'_4Fe_4(CO)_6P_8$ (1) and $Cp'_4Fe_6(CO)_{13}P_8$ (2).** The monoclinic unit cell ($P2_1/c$) of **1** contains four crystallographically related, discrete molecules which pack with no abnormally short intermolecular contacts. The molecular configuration of **1** consists of a $P_8$ cage core with two chelating $\mu_2$-FeCp'(CO) and two terminal $FeCp'(CO)_2$ ligands. Figure 4 presents the labeling of the primary atoms in **1**, and the two views shown emphasize the geometry of the $P_8$ core and the coordination of its organoiron substituents. Although **1** has no crystallographically imposed symmetry, the $P_8$ cage conforms closely to $C_{2v}$-2*mm* symmetry with the $C_2$ axis orthogonal to, and the two vertical mirror planes coincident with, the P1–P2 and P3–P4 bonds. The organoiron ligands reduce the pseudomolecular symmetry to $C_2$-2.

**Table II.** Selected Interatomic Distances and Bond Angles for $Cp'_4Fe_4(CO)_6P_8$ (**1**)

A. Interatomic Distances (Å)

| | | | |
|---|---|---|---|
| P(1)–P(2) | 2.241 (2) | P(1)–P(5) | 2.227 (2) |
| P(1)–P(7) | 2.211 (2) | P(2)–P(6) | 2.234 (2) |
| P(2)–P(8) | 2.210 (2) | P(3)–P(4) | 2.245 (2) |
| P(3)–P(6) | 2.231 (2) | P(3)–P(7) | 2.212 (2) |
| P(4)–P(5) | 2.216 (2) | P(4)–P(8) | 2.226 (2) |
| Fe(1)–P(5) | 2.337 (1) | Fe(1)–P(7) | 2.255 (1) |
| Fe(2)–P(7) | 2.295 (1) | Fe(3)–P(6) | 2.312 (2) |
| Fe(3)–P(8) | 2.243 (1) | Fe(4)–P(8) | 2.309 (1) |
| Fe(1)–C(11) | 1.733 (5) | Fe(1)–Cp(11) | 2.132 (6) |
| Fe(1)–Cp(12) | 2.115 (5) | Fe(1)–Cp(13) | 2.098 (5) |
| Fe(1)–Cp(14) | 2.090 (6) | Fe(1)–Cp(15) | 2.097 (6) |
| Fe(2)–C(21) | 1.773 (6) | Fe(2)–C(22) | 1.751 (6) |
| Fe(2)–Cp(21) | 2.129 (6) | Fe(2)–Cp(22) | 2.114 (6) |
| Fe(2)–Cp(23) | 2.104 (6) | Fe(2)–Cp(24) | 2.119 (5) |
| Fe(2)–Cp(25) | 2.093 (5) | Fe(3)–C(31) | 1.749 (5) |
| Fe(3)–Cp(31) | 2.155 (6) | Fe(3)–Cp(32) | 2.125 (6) |
| Fe(3)–Cp(33) | 2.094 (7) | Fe(3)–Cp(34) | 2.102 (6) |
| Fe(3)–Cp(35) | 2.113 (6) | Fe(4)–C(42) | 1.746 (7) |
| Fe(4)–C(41) | 1.763 (6) | Fe(4)–Cp(41) | 2.112 (6) |
| Fe(4)–Cp(42) | 2.115 (6) | Fe(4)–Cp(43) | 2.107 (6) |
| Fe(4)–Cp(44) | 2.105 (6) | Fe(4)–Cp(45) | 2.107 (6) |
| C(11)–O(11) | 1.157 (6) | C(21)–O(21) | 1.148 (7) |
| C(22)–O(22) | 1.155 (7) | C(31)–O(31) | 1.155 (6) |
| C(42)–O(42) | 1.153 (8) | C(41)–O(41) | 1.157 (7) |

B. Bond Angles (deg)

| | | | |
|---|---|---|---|
| P(1)–P(7)–P(3) | 100.0 (1) | P(1)–P(5)–P(4) | 97.8 (1) |
| P(1)–P(2)–P(6) | 105.9 (1) | P(1)–P(2)–P(8) | 104.8 (1) |
| P(2)–P(6)–P(3) | 97.5 (1) | P(2)–P(8)–P(4) | 99.6 (1) |
| P(2)–P(1)–P(5) | 105.6 (1) | P(2)–P(1)–P(7) | 104.7 (1) |
| P(3)–P(4)–P(5) | 101.5 (1) | P(3)–P(4)–P(8) | 95.0 (1) |
| P(4)–P(3)–P(6) | 101.1 (1) | P(4)–P(3)–P(7) | 94.9 (1) |
| P(5)–P(1)–P(7) | 80.8 (1) | P(5)–P(4)–P(8) | 100.2 (1) |
| P(6)–P(2)–P(8) | 80.4 (1) | P(6)–P(3)–P(7) | 100.6 (1) |
| P(5)–Fe(1)–P(7) | 77.6 (1) | P(6)–Fe(3)–P(8) | 78.1 (1) |
| Fe(1)–P(7)–Fe(2) | 124.4 (1) | Fe(3)–P(8)–Fe(4) | 123.5 (1) |
| Fe(1)–P(5)–P(1) | 90.0 (1) | Fe(1)–P(5)–P(4) | 100.2 (1) |
| Fe(1)–P(7)–P(1) | 92.5 (1) | Fe(1)–P(7)–P(3) | 106.5 (1) |
| Fe(2)–P(7)–P(3) | 112.1 (1) | Fe(2)–P(7)–P(1) | 117.5 (1) |
| Fe(3)–P(6)–P(2) | 90.0 (1) | Fe(3)–P(6)–P(3) | 101.0 (1) |
| Fe(3)–P(8)–P(2) | 92.4 (1) | Fe(3)–P(8)–P(4) | 106.8 (1) |
| Fe(4)–P(8)–P(2) | 117.7 (1) | Fe(4)–P(8)–P(4) | 112.8 (1) |
| P(5)–Fe(1)–C(11) | 93.5 (2) | P(7)–Fe(1)–C(11) | 93.6 (2) |
| P(7)–Fe(2)–C(21) | 88.7 (2) | P(7)–Fe(2)–C(22) | 90.0 (2) |
| C(21)–Fe(2)–C(22) | 93.2 (3) | P(6)–Fe(3)–C(31) | 91.6 (2) |
| P(8)–Fe(3)–C(31) | 91.1 (2) | P(8)–Fe(4)–C(42) | 88.7 (2) |
| P(8)–Fe(4)–C(41) | 89.6 (2) | C(42)–Fe(4)–C(41) | 94.2 (3) |

The monoclinic unit cell ($P2_1/c$) of **2** also contains four crystallographically related molecules with no unusually small intermolecular contacts. Figure 5 provides two views of the molecular geometry of **2**. Formation of the diiron bridge between P6 and P7 occurs when one of two $Fe(CO)_4$ adducts loses one CO and concomitantly forms an Fe–Fe bond with the adjacent $FeCp'(CO)_2$ ligand. This bidentate $(CO)_3Fe(\mu_2\text{-}CO)FeCp'(CO)$ ligand has an Fe–Fe bond length of 2.706 (2) Å, which is within the range for a single-bond interaction. Fe6 of the $Fe(CO)_4$ adduct retains its trigonal-bipyramidal coordination; P5 replaces an apical CO ligand, as is normal for CO substitution reactions. Although **2** has only $C_1$-1 symmetry, its $P_8$ core approximately conforms to $C_s$-*m* symmetry with the mirror plane passing through the P3–P4 bond.

**Bonding Analysis of the $P_8$ Cores of $Cp'_4Fe_4(CO)_6P_8$ (1) and $Cp'_4Fe_6(CO)_{13}P_8$ (2).** Both **1** and **2** possess a $P_8$ core with organoiron ligands. This $P_8$ cage, designated here as $\alpha$-$P_8$, has an open-edged cuneane geometry,[27] which is closely related to the

(27) Cassar, L.; Eaton, P. E.; Halpern, J. *J. Am. Chem. Soc.* **1970**, *92*, 6366. The name "cuneane", coined specifically for pentacyclo-[3.3.0.0$^{2,4}$.0$^{3,7}$.0$^{6,8}$]octane, means wedged-shaped. By opening the 2,4 and 6,8 zero bridges, one forms a compound with tetracyclic open-edged cuneane geometry.

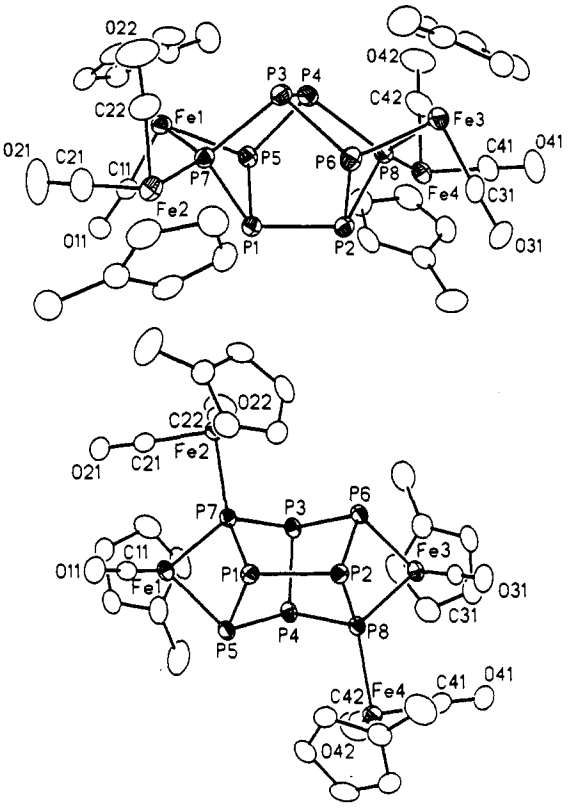


**Figure 4.** Two views of $Cp'_4Fe_4(CO)_6P_8$ (**1**) which has no crystallographically imposed symmetry but which experimentally conforms to $C_2$-2 symmetry. Atomic thermal ellipsoids are drawn at the 30% probability level.

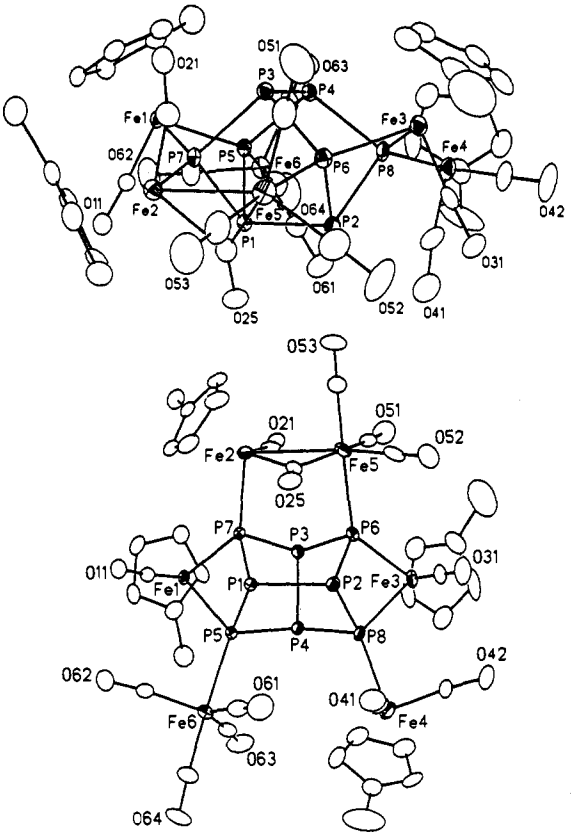


**Figure 5.** Two views of $Cp'_4Fe_6(CO)_{13}P_8$ (**2**) which has no crystallographically imposed symmetry. Atomic thermal ellipsoids are drawn at the 30% probability level.

realgar-type $D_{2d}$-$\bar{4}2m$ geometry. To the best of our knowledge, these two compounds are the first transition-metal complexes containing this $P_8$ cage unit.

This configuration of the $P_8$ cage, formally $\alpha$-$P_8^{4-}$, with eight vertices and ten P–P single bonds, requires 44 valence electrons.[28] In both **1** and **2**, the two 15-electron $\mu_2$-FeCp'(CO) groups are endo-linked to opposite pairs of planar phosphorus atoms, with the iron atoms acting as single-atom bridges across the open phosphorus edges. Each $\mu_2$-iron atom (Fe1 or Fe3) donates one electron in forming an Fe–P single bond with one phosphorus atom (P5 or P6, respectively) and accepts two electrons in forming a dative Fe–P single bond with the other two phosphorus atoms (P7 or P8, respectively). Each iron (Fe2 or Fe4) in the two exo-coordinated 17-electron $FeCp'(CO)_2$ groups donates one electron to a shared-pair single bond with P7 or P8, respectively. Thus, each of the four iron atoms donates one valence electron to the 40-electron $P_8$ core to satisfy the 44 valence electron count required for the open-edged cuneane configuration while attaining its own 18-electron count.

The 44 valence electron count is maintained in **2** because Fe6 and Fe5 are simply Lewis acid $Fe(CO)_4$ and $Fe(CO)_3$ adducts to the lone electron pairs of P5 and P6, respectively, and, as such, contribute no electrons to the $P_8$ core. A closed-shell 18-electron configuration is achieved for Fe5 via its Fe–Fe single bond and shared $\mu_2$-CO ligand with Fe2.

**Syntheses and Spectral-Electrochemical Properties of $Cp'_4Fe_4(CO)_6P_8$ (1) and $Cp'_4Fe_6(CO)_{13}P_8$ (2). (a) Photolytic Generation of $Cp'_4Fe_4(CO)_6P_8$ (1).** This compound was an unanticipated product of the cophotolysis of $[Cp'Fe(CO)_2]_2$ and $P_4$. A similar reaction using $[Cp^*Fe(CO)_2]_2$ (where Cp* denotes $\eta^5$-$C_5Me_5$) had resulted in the formation of $Cp^*FeP_5$,[12d,20a] $[Cp^*FeP_2]_2$,[20a] and other incompletely characterized products, with no evidence for the formation of any complex analogous to **1**. Likewise, in this reaction with $[Cp'Fe(CO)_2]_2$, there is no indication of the formation of either $Cp'FeP_5$ or $[Cp'FeP_2]_2$. Thermal reactions between organometallic complexes and $P_4$ have generally produced metal-coordinated $P_2$ and $P_3$–$P_6$ ring systems[12,16] and a few cubane-like $M_4P_4$ structures[13b,d,29] without the degree of phosphorus clustering found in **1**. Thus, **1**, with its tetracyclicphosphido $P_8$ cage coordinated to transition-metal ligands, is a unique type of metal–polyphosphide complex.

**(b) Generation of $Cp'_4Fe_6(CO)_{13}P_8$ (2) from $Cp'_4Fe_4(CO)_6P_8$ (1) via $Fe(CO)_4$ Fragment Addition.** A primary goal of this reaction was to determine the preferred sites of adduct coordination in **1**. Six of the phosphorus atoms in its $P_8$ core possess a nonbonding electron pair available for coordination with electron-deficient metal fragments. However, the bridgehead atoms (P1, P2, P3, and P4) are all sheltered by the Cp' groups; space-filling models of **1** show conclusively that the planar positions of P5 and P6 are less sterically hindered. Charge distribution calculations on a realgar-type homoatomic system[30] also show that the four atoms at the corners of the square plane are negatively charged with respect to the bridgehead pairs above and below, suggesting that these planar atoms are more susceptible to electrophilic attack. However, this site-preference argument does not take into account any influence that the organoiron substituents in **1** would have on the charge distribution patterns of the $P_8$ core.

While there are numerous accounts of metal fragment addition to bare-phosphido complexes, none of the adducts used, such as $M(CO)_5$ (M = Cr, Mo, W)[31] and $Cp'Mn(CO)_2$,[31c] has either

(28) (a) Wade, K. *Adv. Inorg. Radiochem.* **1976**, *18*, 1. (b) Wade, K. *J. Chem. Soc., Chem. Commun.* **1971**, 792. (c) Mingos, D. M. P. *Acc. Chem. Res.* **1984**, *17*, 311. (d) Mingos, D. M. P. *Nature (London), Phys. Sci.* **1972**, *236*, 99. (e) Lauher, J. W. *J. Am. Chem. Soc.* **1978**, *100*, 5305.

(29) (a) Scherer, O. J.; Braun, J.; Wolmershäuser, G. *Chem. Ber.* **1990**, *123*, 471. (b) Scherer, O. J.; Dave, T.; Braun, J.; Wolmershäuser, G. *J. Organomet. Chem.* **1988**, *350*, C20. (c) Scherer, O. J.; Swarowsky, H.; Wolmershäuser, G.; Kaim, W.; Kohlmann, S. *Angew. Chem., Int. Ed. Engl.* **1987**, *26*, 1153.

(30) Girmac, B. M.; Ott, J. J. *J. Am. Chem. Soc.* **1986**, *108*, 4298.

reacted further to form metal–metal bonds or become involved in more complicated metal–phosphorus shared-pair bonding. However, in situ generated $Fe(CO)_4$ adducts have been found to decarbonylate to $Fe(CO)_3$ and $Fe(CO)_2$, which form metal–metal bonds in certain organometallic sulfido systems.[32] Therefore, $Fe(CO)_4$, generated from $Fe(CO)_5/Me_3NO$ or $Fe_2(CO)_9$, was chosen as a potential adduct with **1** based on the premise that its facile decarbonylation could result in metal–metal bond formation.

As was anticipated, the $Fe(CO)_4$ fragments coordinated to the planar P5 and P6 atoms, and an iron–iron bond was formed. Less readily anticipated was the absence of any additional complexation to the bridgehead atoms, even in the presence of a large excess of the adduct, and the formation of only one metal–metal bond leading to the observed structure of **2**. Formation of the Fe2–Fe5 bond formally involves (1) loss of one CO from either of the two $Fe(CO)_4$ adducts with (2) concomitant electron-pair Fe–Fe bonding and bridging carbonyl linkage of the adjacent $FeCp'(CO)_2$ terminal ligand with the resulting $Fe(CO)_3$ fragment. Figure 5 illustrates how the distortion of the $P_8$ core, produced by this two-iron bridge between P7 and P8, then forces the remaining $Fe(CO)_4$ and $FeCp'(CO)_2$ groups to be too far apart for a second Fe–Fe bonding interaction to occur.

**(c) Infrared Spectral Analysis.** Solid-state infrared spectra of **1** and **2** are in accordance with their configurations as established by the X-ray diffraction studies. A spectrum of **1** shows only three terminal carbonyl absorption bands from the two sets of 2-fold-related groups, $FeCp'(CO)_2$ and $\mu_2$-$FeCp'(CO)$. A spectrum of **2** exhibits numerous terminal carbonyl bands due to these same groups and the $Fe(CO)_x$ adducts ($x$ = 3, 4). A lower band at 1755 $cm^{-1}$ is assigned to the bridging carbonyl spanning the Fe2–Fe5 bond.

**(d) NMR Spectral Analysis.** The $^{31}P$ NMR spectra for **1** and **2** are given in Figure 1. The $C_2$ geometry of **1** and the approximate $C_{2v}$ configuration of its $P_8$ core result in the eight phosphorus nuclei conforming to an AA'BB'MM'XX' (P1/P2, P3/P4, P5/P6, P7/P8) spin system with intrinsically second-order coupling interactions. These interactions effectively preclude a determination of coupling constants from the spectrum. However, the geometrical and chemical similartiy of the P1/P2 and P3/P4 pairs under the idealized $C_{2v}$ core symmetry suggests that they may exhibit similar chemical shift properties as well. Therefore, the very closely spaced, complex signals at $\delta$ 119 and 121 ppm may be assigned with reasonable confidence to these two bridgehead atom pairs. It is a common observation that metal–phosphorus bonding tends to shift the phosphorus resonances upfield. Since P7 and P8 are each bonded to two iron atoms, the high field signal at $\delta$ 82 ppm is tentatively assigned to this P7/P8 atom pair. The low field resonance at $\delta$ 138 ppm is then assigned to the remaining P5/P6 atom pair. Unfortunately, due to the extensive coupling among the phosphorus nuclei, it is not possible to confirm these assignments. A COSY spectrum, for instance, would show cross peaks between every pair of $^{31}P$ resonances and, thus, would provide no distinction among them. Multiple quantum filtered experiments would be similarly uninformative.

As in **1**, the homogeneous phosphorus composition of the core and the absence of other NMR-active nuclei prevent unambiguous signal assignments in **2**. However, a certain amount of information can still be extracted from the $^{31}P$ spectrum (Figure 1b). First, the spectrum establishes that the $C_1$ symmetry of the molecule is also present in solution. Thus, no significant molecular or cage fluctuations, which would change the average core geometry, are evident. Second, the general downfield shift of resonances relative to those in **1** is consistent with the anticipated inductive effects of the electron-withdrawing $Fe(CO)_x$ adducts ($x$ = 3, 4) upon the $P_8$ core.

Despite the reduced symmetry, the P1/P2 and P3/P4 pairs of bridgehead atoms of **2** are still very nearly geometrically and chemically similar as was found in **1**. The two complex signals at $\delta$ 147 and 154 ppm in **2**, which are virtually identical with the signals at $\delta$ 119 and 121 ppm in **1**, are then assigned to these two quasi-sets. These chemical shift values are approximately 30 ppm downfield from the comparable signals in **1**. The extent of this shift suggests that the electronic environments of the bridgehead atoms are strongly influenced by the $Fe(CO)_x$ ($x$ = 3, 4) groups on the adjacent phosphorus atoms P5 and P6.

Additional spectral assignments may be made which, while not absolute, are consistent with the structure of **2**. The two low field resonances at $\delta$ 169 and 186 ppm are again assigned to P5 and P6 with no further discrimination. Validation of this choice is provided by the large downfield shift of these resonances from $\delta$ 138 ppm found in **1**. The direction of this shift is consistent with the deshielding effects expected from direct coordination of electron-withdrawing $Fe(CO)_x$ ($x$ = 3, 4) adducts to these nuclei. The two high field resonances, $\delta$ 75 and 123 ppm, are assigned to the remaining atoms P7 and P8. Since the chemical environment of P8 in **2** is virtually the same as in **1**, the signal at $\delta$ 75 ppm is assigned to this atom. The remaining signal at $\delta$ 123 ppm is assigned to P7 whose $FeCp'(CO)_2$ substituent is additionally bonded to Fe5.

The $^{31}P$ NMR signals of the planar phosphorus atoms (P5, P6, P7, and P8) exhibit some unusual and intriguing first-order resonance couplings. Each of these four phosphorus nuclei would be expected to show two large couplings with the two nuclei to which each is directly bonded. However, the signals at $\delta$ 75 and 123 ppm assigned to P7 and P8, respectively, each show *three* large couplings. The signal at $\delta$ 75 (d/t, $J_{(P-P)}$ = 343/294 Hz) ppm is very nearly a quartet as is found at $\delta$ 123 (q, $J_{(P-P)}$ = 343 Hz) ppm and has the same large coupling constant. Because the P5 and P6 resonances show splittings only for their one-bond partners, we conclude that a remarkably large three-bond coupling of 343 Hz between P7 and P8, the same as their one-bond couplings, is responsible for this third coupling. In fact, for P8 this three-bond coupling is the largest observed splitting, nearly 50 Hz larger than the two one-bond couplings.

A summary of this tentative $^{31}P$ spectral assignment for **2** is $\delta$ 75 (P8), 123 (P7), 147 (P1/P2 or P3/P4), 154 (P1/P2 or P3/P4), 169 (P5 or P6), and 186 (P5 or P6) ppm.

The proton NMR spectra of **1** and **2** are in accordance with their solid-state pseudo-$C_2$ and $C_1$ geometries, respectively, being unchanged in solution.

**(e) Mass Spectral Analysis.** Positive- and negative-ion LD/FT mass spectra of compounds **1** and **2** are presented in Figures 2 and 3. Assignments for selected ion peaks are given in the relevant Experimental Section, and a more complete list of ion-peak assignments is available as supplementary material. In addition to these mass spectra providing a substantiation of the elemental compositions of these two compounds, two important pieces of structural information can be derived from the fragmentation patterns. First, both compounds exhibit a number of relatively abundant $P_8$-containing ion peaks. Thus, it would appear that there is no inherent fragility of the $P_8$ cage in **1** and **2**. Second, all observed ion peaks assigned to $P_8$-containing fragments possess, without exception, at least two coordinated FeCp' groups. Given the observation that loss of the one or two FeCp' ligands does not affect the number of $P_8$-containing fragments but the loss of more than two does, we conclude that the two chelating $\mu_2$-FeCp' units found in each compound are essential to $P_8$-cage stabilization.

Ion-peak assignment for **1** is simplified by the fact that every iron atom is bonded to one methylcyclopentadienyl ligand, which remains firmly attached in all observed fragments. In **2**, however, the two $Fe(CO)_x$ adducts cause ambiguity in some ion-peak assignments since the mass of one Fe (56 amu) atom is approximately the same as the mass of two CO units (2 × 28 amu). Thus, virtually all of the $P_8$-containing ion peaks can be given multiple assignments, and some signals may actually be produced by several ions with very similar mass and charge. However, in most cases the bonding interactions within the molecule suggest a preferred ion-peak interpretation. For example, negative-ion peaks at $m/z$

(31) (a) Goh, L. Y.; Wong, R. C. S.; Mak, T. C. W. *J. Organomet. Chem.* **1989**, *364*, 363. (b) Scherer, O. J.; Sitzmann, H.; Wolmershäuser, G. *Angew. Chem., Int. Ed. Engl.* **1984**, *23*, 968. (c) Scherer, O. J.; Schwalb, J.; Wolmershäuser, G. *New J. Chem.* **1989**, *13*, 399.

(32) Brunner, H.; Janietz, N.; Wachter, J.; Zahn, T.; Ziegler, M. L. *Angew. Chem., Int. Ed. Engl.* **1985**, *24*, 133.

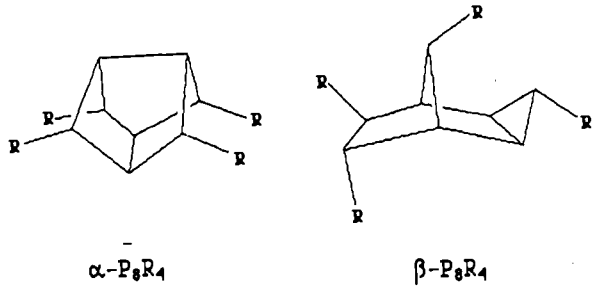


**Figure 6.** The two isomeric configurations found for $P_8R_4$ (where R = iPr) whose $P_8$ cores were deduced from $^{31}P$ NMR measurements by Baudler et al.[37] The thermodynamically unstable $\alpha$-$P_8R_4$ isomer is structurally analogous to realgar; the thermodynamically favored $\beta$-$P_8R_4$ isomer is geometrically similar to norborane.

765 and 709 are observed in the mass spectra of both **1** and **2**, but they have been assigned to different ions because of the different fragmentation patterns expected from the bonding in each molecule.

**(f) Electrochemical Analysis.** Cyclic voltammograms for **1** and **2** do not exhibit any reversible redox couples within the observed range of +1.8 to −2.1 V. **1** shows a quasi-reversible couple at $E_{1/2}$ = 0.34 V in $CH_2Cl_2$, which approaches reversibility only at higher scan speeds (>500 mV/s). Additional irreversible oxidations occur at $E_p$ = 0.73 and 0.89 V, while an irreversible reduction occurs at $E_p$ = −1.49 V. In $CH_3CN$, all redox behavior appears irreversible at 200 mV/s with oxidation waves at $E_p$ = 0.38 and 0.55 V and reduction waves at $E_p$ = −0.98 and −1.45 V. **2** also exhibits only nonreversible redox behavior. In THF, **2** has oxidation waves at $E_p$ = 0.42, 0.52, and 0.75 V, while reduction waves are observed at $E_p$ = −1.02 and −1.36 V.

**Structural Analysis of the $P_8$ Cages of $Cp'_4Fe_4(CO)_6P_8$ (1) and $Cp'_4Fe_6(CO)_{13}P_8$ (2) and Comparisons with Analogous Systems.** $\alpha$-$P_8$ cages appear to be thermally unstable unless coordinated to bridging ligands. Although salts of $P_7^{3-}$, $P_{11}^{3-}$, and other polyphosphide anions[4] have been prepared, no salts containing the $P_8^{4-}$ anion have yet been isolated. Even octaphosphorus tetrahydride, $P_8H_4$, has been identified solely by mass spectrometry.[33] Given the idealized $D_{2d}$-$\bar{4}2m$ geometry of the $\alpha$-$P_8$ cage, it is most likely that unfavorable steric interactions between endo-oriented sets of planar phosphorus orbitals account for much of this apparent instability of the anion.

An abnormally long P–P bond length in the isostructural, isoelectronic $\alpha$-$P_4S_4$ molecule[34] (**5**) indicates that electron-pair repulsions between nonbonding orbitals of the bridgehead atoms may be an additional destabilizing factor. In the $D_{2d}$ configuration of $P_4S_4$, the phosphorus atoms are in the bridgehead positions with their nonbonding electron pairs held in a rigidly eclipsed arrangement. Thus, it is reasonable to presume that the long P–P bond, which at 2.35 Å is much longer than a normal P–P single bond of ~2.23 Å (e.g., orthorhombic phosphorus),[35] is a consequence of orbital steric repulsions.

Alkylated complexes, $P_8R_4$, would have enhanced bridgehead and planar orbital repulsions within the $\alpha$-$P_8$ framework. Hence, it is not surprising that the few alkyl derivatives of $\alpha$-$P_8R_4$ (R = Me, Et, iPr) prepared by Baudler and co-workers[36] are formed in low yields and are thermally unstable. Extensive work by Baudler et al.[37] with polycyclicphosphanes led to their hypothesis that the $\alpha$-$P_8$ core configuration must be stabilized by incorporation into a larger $P_n$ framework. This proposal was based partly on the facile, irreversible isomerization of $\alpha$-$P_8(iPr)_4$ to $\beta$-$P_8(iPr)_4$ under thermal reaction conditions (Figure 6). They reported MNDO calculations on a simplified $P_8Me_4$ model which indicate, for these nonbridged systems, that the $\beta$-$P_8$ norborane isomer is more stable than the $\alpha$-$P_8$ isomer by 4.3 kcal/mol.[37] In contrast, Hittorf's phosphorus[38] (**3**) and $\alpha$-$P_8(P_2iPr_2)_2$[39] (**4**), which have their $\alpha$-$P_8$ cores rigidly held by bridging $P_2$ units, are relatively thermally stable. Other $P_n$ structures containing realgar-type $\alpha$-$P_8$ cages stabilized by chelating $\mu_2$-$P_2$ fragments[4b] include tubular $^1_\infty(P_{12})$ neutral units with alternating $P_8$ cages and planar $P_4$ rings found in the structurally unique $Cu_2P_3I_2$ and the tubular $^1_\infty(P_{15})^-$ monoanion composed of alternating $\alpha$-$P_8$ and norborane-type $P_7^-$ cages. Indeed, it appears that only chelating ligands, such as $P_2$ fragments or the $\mu_2$-Fe atoms in **1** and **2**, are able to minimize the steric repulsions inherent between the tetrahedrally coordinated planar atoms in the $\alpha$-$P_8$ cage. Except for the aforementioned alkyl systems, the $\alpha$-$P_8$ unit has previously been found only as subunits of rigid $P_n$ frameworks.

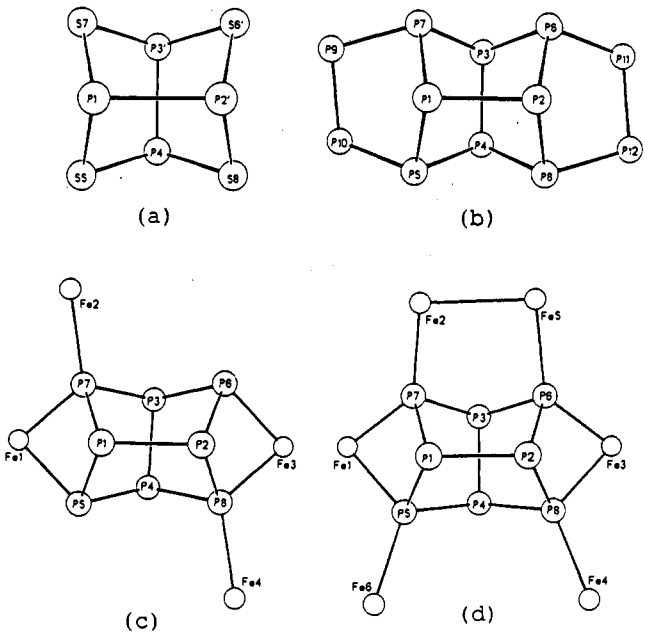


**Figure 7.** Geometries are as follows: (a) $\alpha$-$P_4S_4$ (**5**) with crystallographic $C_2$-2 site symmetry and pseudo-$D_{2d}$-$\bar{4}2m$ symmetry. (b) $\alpha$-$P_8$ subunit with two $\mu_2$-$P_2$ bridges found in Hittorf's phosphorus allotrope (**3**). The $P_8(P_2)_2$ fragment closely conforms to $C_{2v}$-$2mm$ symmetry. A nearly identical $P_8(P_2)_2$ framework is found in $P_8(P_2iPr_2)_2$ (**4**). (c) $\alpha$-$P_8$ cage and coordinated iron atoms of $Cp'_4Fe_4(CO)_6P_8$ (**1**). The $P_8$ core exhibits pseudo $C_{2v}$-$2mm$ symmetry; inclusion of all atoms reduces the pseudosymmetry to $C_2$-2. (d) $\alpha$-$P_8$ cage and coordinated iron atoms of $Cp'_4Fe_6(CO)_{13}P_8$ (**2**). The $P_8$ core exhibits pseudo-$C_s$-$m$ symmetry; inclusion of all atoms reduces the symmetry to $C_1$-1.

Table IV and Figure 7 summarize the specific atoms, bonds, and angles for the compounds in the following discussion. Hittorf's phosphorus allotrope (**3**) contains alternating $P_8$ and $P_9$ units linked by $P_2$ chelating bridges.[35,38] In the $\alpha$-$P_8$ unit of interest, the bridged P5/P7 and P6/P8 pairs at 3.37 Å (av) are only 0.37 Å farther apart than the nonbridged P5/P8 and P6/P7 pairs. Thus, the two-atom $P_2$ bridges induce minimal distortion on the $P_8$ cage from its idealized nonbridged $D_{2d}$ geometry. The P1–P2 and P3–P4 bridgehead bonds in this compound are 0.08 Å longer than the mean of its other P–P bonds. As noted by Thurns and Krebs,[38b] this longer bond length is consistent with the need to reduce electronic interactions between the nonbonding eclipsed orbitals (torsion angles = −0.3, 0.0°). This repulsion argument is also used to explain a similar lengthening of the bridgehead bonds in **4**,[39b] whose $P_8$ core and $P_{12}$ framework are virtually identical with

(33) Baudler, M.; Standeke, H.; Borgardt, M.; Strabel, H.; Dobbers, J. *Naturwissenschaften* **1966**, *53*, 106.
(34) (a) Griffin, A. M.; Minshall, P. C.; Sheldrick, G. M. *J. Chem. Soc., Chem. Commun.* **1976**, 809. (b) Chang, C.-C.; Haltiwanger, R. C.; Norman, A. D. *Inorg. Chem.* **1978**, *17*, 2056.
(35) Donohue, J. *Structure of the Elements*; J. Wiley & Sons: New York, 1974; pp 289–295.
(36) Baudler, M.; Arndt, V. *Z. Naturforsch.* **1984**, *B39*, 275.
(37) Baudler, M.; Koll, B.; Adamek, C.; Gleiter, R. *Angew. Chem., Int. Ed. Engl.* **1987**, *26*, 347.
(38) (a) Thurn, H.; Krebs, H. *Angew. Chem., Int. Ed. Engl.* **1966**, *5*, 1047. (b) Thurn, H.; Krebs, H. *Acta. Crystallogr.* **1969**, *B25*, 125.
(39) (a) Baudler, M.; Aktalay, Y.; Arndt, V.; Tebbe, K.-F.; Feher, M. *Angew. Chem., Int. Ed. Engl.* **1983**, *22*, 1022. (b) Tebbe, K.-F.; Feher, M. *Z. Naturforsch.* **1986**, *B41*, 548.

**Table III.** Selected Interatomic Distances and Bond Angles for $Cp'_4Fe_6(CO)_{13}P_8$ (**2**)

A. Interatomic Distances (Å)

| | | | | | | | |
|---|---|---|---|---|---|---|---|
| P(1)–P(2) | 2.220 (4) | P(1)–P(5) | 2.225 (4) | Fe(3)–Cp(32) | 2.108 (16) | Fe(3)–Cp(33) | 2.073 (13) |
| P(1)–P(7) | 2.206 (4) | P(2)–P(6) | 2.226 (5) | Fe(3)–Cp(34) | 2.086 (14) | Fe(3)–Cp(35) | 2.086 (17) |
| P(2)–P(8) | 2.209 (4) | P(3)–P(4) | 2.223 (4) | Fe(4)–C(41) | 1.685 (17) | Fe(4)–C(42) | 1.755 (14) |
| P(3)–P(6) | 2.185 (4) | P(3)–P(7) | 2.196 (4) | Fe(4)–Cp(41) | 2.101 (15) | Fe(4)–Cp(42) | 2.057 (16) |
| P(4)–P(5) | 2.251 (4) | P(4)–P(8) | 2.254 (4) | Fe(4)–Cp(43) | 2.119 (17) | Fe(4)–Cp(44) | 2.111 (15) |
| Fe(2)–Fe(5) | 2.706 (2) | Fe(1)–P(5) | 2.292 (3) | Fe(4)–Cp(45) | 2.087 (13) | Fe(5)–C(25) | 1.919 (13) |
| Fe(1)–P(7) | 2.227 (3) | Fe(2)–P(7) | 2.253 (3) | Fe(5)–C(51) | 1.824 (16) | Fe(5)–C(52) | 1.782 (16) |
| Fe(3)–P(6) | 2.219 (3) | Fe(3)–P(8) | 2.278 (4) | Fe(5)–C(53) | 1.804 (14) | Fe(6)–C(61) | 1.785 (15) |
| Fe(4)–P(8) | 2.298 (4) | Fe(5)–P(6) | 2.343 (3) | Fe(6)–C(62) | 1.804 (13) | Fe(6)–C(63) | 1.756 (17) |
| Fe(6)–P(5) | 2.315 (3) | Fe(1)–C(11) | 1.714 (12) | Fe(6)–C(64) | 1.779 (15) | C(11)–O(11) | 1.187 (14) |
| Fe(1)–Cp(11) | 2.142 (14) | Fe(1)–Cp(12) | 2.105 (13) | C(21)–O(21) | 1.163 (18) | C(25)–O(25) | 1.166 (17) |
| Fe(1)–Cp(13) | 2.102 (14) | Fe(1)–Cp(14) | 2.088 (14) | C(31)–C(31) | 1.170 (17) | C(41)–O(41) | 1.179 (21) |
| Fe(1)–Cp(15) | 2.103 (13) | Fe(2)–C(21) | 1.746 (15) | C(42)–O(42) | 1.163 (17) | C(51)–O(51) | 1.153 (20) |
| Fe(2)–C(25) | 2.021 (13) | Fe(2)–Cp(21) | 2.141 (12) | C(52)–O(52) | 1.149 (20) | C(53)–O(53) | 1.148 (17) |
| Fe(2)–Cp(22) | 2.122 (12) | Fe(2)–Cp(23) | 2.131 (13) | C(61)–O(61) | 1.162 (19) | C(62)–O(62) | 1.141 (17) |
| Fe(2)–Cp(24) | 2.080 (13) | Fe(2)–Cp(25) | 2.087 (13) | C(63)–O(63) | 1.161 (20) | C(64)–O(64) | 1.147 (19) |
| Fe(3)–C(31) | 1.726 (14) | Fe(3)–Cp(31) | 2.062 (17) | | | | |

B. Bond Angles (deg)

| | | | | | | | |
|---|---|---|---|---|---|---|---|
| P(1)–P(5)–P(4) | 98.7 (2) | P(1)–P(2)–P(6) | 103.0 (2) | P(7)–Fe(2)–C(25) | 87.4 (3) | C(21)–Fe(2)–C(25) | 113.1 (6) |
| P(1)–P(2)–P(8) | 108.0 (2) | P(1)–P(7)–P(3) | 101.2 (2) | P(6)–Fe(3)–C(31) | 92.2 (4) | P(8)–Fe(3)–C(31) | 93.5 (4) |
| P(2)–P(6)–P(3) | 100.6 (2) | P(2)–P(8)–P(4) | 99.1 (2) | P(8)–Fe(4)–C(41) | 90.9 (5) | P(8)–Fe(4)–C(42) | 92.0 (5) |
| P(2)–P(1)–P(5) | 108.2 (2) | P(2)–P(1)–P(7) | 101.8 (2) | C(41)–Fe(4)–C(42) | 92.7 (8) | Fe(2)–Fe(5)–C(25) | 48.2 (4) |
| P(3)–P(4)–P(5) | 94.8 (1) | P(3)–P(4)–P(8) | 94.3 (2) | P(6)–Fe(5)–C(25) | 85.0 (4) | Fe(2)–Fe(5)–C(51) | 113.2 (4) |
| P(4)–P(3)–P(6) | 100.3 (2) | P(4)–P(3)–P(7) | 100.3 (2) | P(6)–Fe(5)–C(51) | 89.4 (4) | C(25)–Fe(5)–C(51) | 159.8 (6) |
| P(5)–P(4)–P(8) | 106.1 (2) | P(5)–P(1)–P(7) | 79.0 (1) | Fe(2)–Fe(5)–C(52) | 142.5 (5) | P(6)–Fe(5)–C(52) | 85.7 (5) |
| P(6)–P(2)–P(8) | 78.0 (1) | P(6)–P(3)–P(7) | 92.7 (2) | C(25)–Fe(5)–C(52) | 94.7 (6) | C(51)–Fe(5)–C(52) | 104.2 (6) |
| P(5)–Fe(1)–P(7) | 77.1 (1) | P(6)–Fe(3)–P(8) | 76.7 (1) | Fe(2)–Fe(5)–C(53) | 86.6 (4) | P(6)–Fe(5)–C(53) | 175.7 (5) |
| Fe(1)–P(7)–Fe(2) | 132.9 (1) | Fe(1)–P(5)–Fe(6) | 123.2 (1) | C(25)–Fe(5)–C(53) | 92.8 (6) | C(51)–Fe(5)–C(53) | 93.8 (6) |
| Fe(3)–P(6)–Fe(5) | 133.7 (1) | Fe(3)–P(8)–Fe(4) | 116.6 (1) | C(52)–Fe(5)–C(53) | 90.7 (7) | P(5)–Fe(6)–C(61) | 87.5 (5) |
| Fe(1)–P(7)–Fe(2) | 132.9 (1) | Fe(1)–P(5)–Fe(6) | 123.2 (1) | P(5)–Fe(6)–C(62) | 90.0 (5) | C(61)–Fe(6)–C(62) | 117.4 (6) |
| Fe(3)–P(6)–Fe(5) | 133.7 (1) | Fe(2)–Fe(5)–P(6) | 94.8 (1) | P(5)–Fe(6)–C(63) | 90.4 (5) | C(61)–Fe(6)–C(63) | 127.7 (6) |
| Fe(5)–Fe(2)–P(7) | 96.8 (1) | Fe(1)–P(5)–P(1) | 90.8 (1) | C(62)–Fe(6)–C(63) | 114.8 (7) | P(5)–Fe(6)–C(64) | 176.4 (5) |
| Fe(6)–P(5)–P(1) | 116.2 (2) | Fe(1)–P(5)–P(4) | 106.1 (2) | C(61)–Fe(6)–C(64) | 89.0 (7) | C(62)–Fe(6)–C(64) | 92.4 (6) |
| Fe(6)–P(5)–P(4) | 116.6 (1) | Fe(3)–P(6)–P(2) | 91.8 (1) | C(63)–Fe(6)–C(64) | 91.0 (7) | Fe(1)–C(11)–O(11) | 174.5 (10) |
| Fe(5)–P(6)–P(2) | 115.6 (2) | Fe(3)–P(6)–P(3) | 104.9 (2) | Fe(2)–C(21)–O(21) | 164.1 (11) | Fe(2)–C(25)–Fe(5) | 86.7 (6) |
| Fe(5)–P(6)–P(3) | 105.5 (2) | Fe(1)–P(7)–P(1) | 93.0 (1) | Fe(2)–C(25)–O(25) | 131.1 (9) | Fe(5)–C(25)–O(25) | 142.1 (10) |
| Fe(2)–P(7)–P(1) | 116.7 (2) | Fe(1)–P(7)–P(3) | 101.6 (1) | Fe(3)–C(31)–O(31) | 176.2 (11) | Fe(4)–C(41)–O(41) | 175.3 (13) |
| Fe(2)–P(7)–P(3) | 106.8 (1) | Fe(3)–P(8)–P(2) | 90.7 (1) | Fe(4)–C(42)–O(42) | 174.5 (12) | Fe(5)–C(51)–O(51) | 175.9 (13) |
| Fe(4)–P(8)–P(2) | 119.3 (2) | Fe(3)–P(8)–P(4) | 108.4 (2) | Fe(5)–C(52)–O(52) | 179.1 (15) | Fe(5)–C(53)–O(53) | 178.2 (15) |
| Fe(4)–P(8)–P(4) | 118.3 (2) | P(5)–Fe(1)–C(11) | 92.8 (4) | Fe(6)–C(61)–O(61) | 178.1 (11) | Fe(6)–C(62)–O(62) | 175.7 (12) |
| P(7)–Fe(1)–C(11) | 92.9 (4) | Fe(5)–Fe(2)–C(21) | 69.1 (4) | Fe(6)–C(63)–O(63) | 177.0 (12) | Fe(6)–C(64)–O(64) | 176.5 (13) |
| P(7)–Fe(2)–C(21) | 90.5 (4) | Fe(5)–Fe(2)–C(25) | 45.1 (4) | | | | |

analogous units in **3** (Figure 7b). The $P_8$ cages of these two compounds closely conform to noncrystallographically imposed $C_{2v}$ symmetry.

In contrast to the two-atom $P_2$ bridges of **3** and **4**, the single-atom $\mu_2$-Fe bridges in **1** are much more structurally constraining. The larger difference in nonbonding P–P distances between the bridged (2.87 Å (av)) and nonbridged (3.42 Å (av)) planar atom pairs[4b] indicates a more severe, but still symmetrical, deformation of the $P_8$ core in **1** from an idealized $D_{2d}$ to $C_{2v}$ geometry. However, since this observed reduction in the Fe-bridged P···P nonbonding distances is balanced by a commensurate increase in the nonbridged P···P distances, the average of these distances in **1** remains nearly identical with the mean P···P distance in the less distorted **3**. In contrast to the relatively long bridgehead P–P bond lengths found in **3**, **4**, and **5**, the bridgehead P1–P2 and P3–P4 bond lengths in **1** are only marginally longer (0.02 Å) than the mean of the remaining P–P bonds. While the nonbonding electron pairs of these atoms are still essentially eclipsed, the torsion angles *have* increased slightly to 2.4 and 4.0°. Although this marginal increase in torsion angle alone may account for part of the relative decrease in the P–P bond lengths, the electronic effects of the iron substituents need to be considered as well (vida infra).

The $P_8$ core of **2** possesses an idealized $C_s$-*m* geometry. The P6–P3–P7 bond angle is decreased by 8° and the P6···P7 nonbonding distance by 0.25 Å from their respective values in **1** due to the additional formation of the $\mu_2$-diiron bridge. One particularly interesting structural feature of **2** is that the 2.706 (2) Å $\mu_2$-$Fe_2$ bridge spans a nonbonding edge of only 3.17 Å, whereas the shorter $\mu_2$-$P_2$ bridges in **3** (2.27 Å) span considerably longer nonbonding edges of 3.37 Å (av). Thus, the $\mu_2$-$Fe_2$ bridge appears to distort the $\alpha$-$P_8$ cage to a much greater extent than is sterically necessary. Space-filling diagrams of **2** show no significant steric interactions between the opposite $CpFe(CO)_2$ and $Fe(CO)_4$ groups. Therefore, it appears that prior electronic and structural constraints upon the $\mu_2$-$Fe_2$ bridged phosphorus atoms introduced by the initial $\mu_2$-$Fe_1$ bridges must account for this anomaly. The core deformation induced by the $\mu_2$-$Fe_2$ bridge is balanced by a commensurate increase in the P5···P8 nonbonding distance to 3.60 Å. Fe4 and Fe6 of the groups attached to P5 and P8 are thus forced far apart (5.08 Å), such that Fe–Fe bonding between these groups is precluded.

In **2**, the P1–P2 and P3–P4 bridgehead bond lengths are virtually identical with the mean of the other eight P–P bonds. However, the torsion angles between the relevant pairs of bridgehead orbitals (0.1° and 0.9°) are comparable to those found in **3** and **5**. A plausible explanation for the absence of any bridgehead bond lengthening is that the inductive effects of the strongly electron-deficient Lewis acid $Fe(CO)_x$ ($x$ = 3, 4) adducts in **2** result in decreased sizes of the eclipsed nonbonding orbitals of bridgehead atoms, thus effectively reducing repulsive interactions between them. That the inductive effect of the $Fe(CO)_x$ adducts influences the bridgehead P atoms is indicated by their $^{31}P$ resonances in **2** being shifted downfield by ~30 ppm from their resonances in **1**.

### Structural–Chemical Conclusions

As shown in Table IV, despite the differences in the type and number of bridging ligands, the *means* of the corresponding P–P bonding and nonbonding P···P distances and of the bridgehead angles are surprisingly similar in the $P_8$ cages of **1**, **2**, and **3**. Thus,

**Table IV.** Selected Interatomic Distances (Å) and Bond Angles (deg) for the $\alpha$-$P_8$ Cores of $Cp'_4Fe_4(CO)_6P_8$ (**1**), $Cp'_4Fe_6(CO)_{13}P_8$ (**2**), Hittorf's Phosphorus (**3**),[a] and $\alpha$-$P_4S_4$ (**5**)[b,c]

| compd | 1 | 2 | 3 | 5 |
|---|---|---|---|---|
| core symmetry | $C_{2v}$ | $C_s$-$m$ | $C_{2v}$ | $D_{2d}$ |
| P1–P2 | 2.241 (2) | 2.220 (4) | 2.299 (3) | 2.353 (1)[c] |
| P3–P4 | 2.245 (2) | 2.223 (4) | 2.285 (3) | 2.353 (1) |
| av | 2.24 | 2.22 | 2.29 | 2.35 |
| P1–P7 | 2.211 (2) | 2.206 (4) | 2.236 (3) | |
| P7–P3 | 2.212 (2) | 2.196 (4) | 2.202 (3) | |
| P3–P6 | 2.231 (2) | 2.185 (4) | 2.201 (3) | |
| P6-P2 | 2.234 (2) | 2.226 (5) | 2.239 (3) | |
| P2–P8 | 2.210 (2) | 2.209 (4) | 2.240 (3) | |
| P8–P4 | 2.226 (2) | 2.254 (4) | 2.205 (3) | |
| P4–P5 | 2.216 (2) | 2.251 (4) | 2.207 (3) | |
| P5–P1 | 2.227 (2) | 2.225 (4) | 2.237 (3) | |
| av | 2.22 | 2.22 | 2.21 | |
| P7···P6 | 3.418 (2) | 3.169 (4) | 3.016 (3) | |
| P6···P8 | 2.869 (2) | 2.791 (4) | 3.370 (3) | |
| P8···P5 | 3.408 (2) | 3.598 (4) | 2.966 (3) | |
| P5···P7 | 2.878 (2) | 2.818 (4) | 3.358 (3) | |
| av | 3.14 | 3.09 | 3.18 | |
| P7–P1–P5 | 80.8 (1) | 79.0 (1) | 97.3 (1) | 95.3 (1) |
| P6–P2–P8 | 80.4 (1) | 78.0 (1) | 97.6 (1) | 95.1 (1)[c] |
| P7–P3–P6 | 100.6 (1) | 92.7 (2) | 86.5 (1) | 95.3 (1)[c] |
| P5–P4–P8 | 100.2 (1) | 106.1 (2) | 84.5 (1) | 95.1 (1) |
| av | 90.5 | 89.0 | 91.5 | 95.2 |
| P1···P4 | 3.349 (2) | 3.393 (4) | 3.380 (3) | |
| P1···P3 | 3.388 (2) | 3.404 (4) | 3.359 (3) | |
| P2···P3 | 3.357 (2) | 3.395 (4) | 3.373 (3) | |
| P2···P4 | 3.389 (2) | 3.395 (4) | 3.389 (3) | |
| av | 3.37 | 3.40 | 3.38 | |

[a] The corresponding P–P distances and P–P–P bond angles for the $\alpha$-$P_8$ core of $P_8(P_2iPr_2)_2$ (**4**) are analogous to those of **3**. [b] Angles given are for positionally analogous P and S atoms. [c] Crystallographically dependent bond lengths and angles.

the $\alpha$-$P_8$ cage exhibits marked flexibility and is able to compensate for a large degree of distortion. Additionally, the two bridgehead P–P units maintain an idealized $D_{2d}$ geometry in each of the compounds **1**–**5**, regardless of the differing cage symmetries engendered by their various bridging substituents. Cage distortions, therefore, appear to affect only the directly coordinated planar phosphorus atoms.

The $\mu_2$-Fe bridges in **1** and **2** are undoubtedly the primary contributors to the stability of their $\alpha$-$P_8$ cores. Evidence of the thermal stability of $\alpha$-$P_8$ core in **1** is given by the observation that refluxing **1** in toluene for 4 h resulted in no detectable reaction—neither isomerization nor decomposition products were formed in measurable quantities. Additionally, an examination of the major mass spectral ions reported above for **1** and **2** reveals that, while there are a number of relatively abundant ion peaks assigned to fragments containing the $P_8$ cage, there are no such ion fragments detected which do not contain at least two FeCp′ groups (no doubt the $\mu_2$-FeCp′ bridging groups) in either compound. Thus, the chelating iron bridges are essential to the structural integrity of the $\alpha$-$P_8$ core in **1** and **2**.

The $\alpha$-$P_8$ cages in **1** and **2** appear to be stabilized not only by the chelating $\mu_2$-Fe bridges but also by their electron-deficient transition-metal adducts. It has been suggested that the lengthed P–P bridgehead bonds in $\alpha$-$P_4S_4$[34a] and $\alpha$-$P_8(iPr)_4$[37] are an indication of bond strain. If this premise is valid, then the relatively short bridgehead bonds in **1** and **2** suggest that the destabilizing repulsive effects of the eclipsed bridgehead nonbonding orbitals, along with resultant bond strain, have been decreased. While the $^{31}P$ NMR spectrum of **2** provides evidence that the $Fe(CO)_x$ adducts ($x$ = 3, 4) exert discernible electron-withdrawing effects on the bridgehead atoms, the electronic effects of the $FeCp'(CO)_x$ ($x$ = 1, 2) groups, found in both **1** and **2**, are not clearcut. Each of these ligands actually donates one electron to the $P_8$ core through a shared-pair single bond. However, the minimal degree of bridgehead bond lengthening found in **1** is consistent with some decrease in electronic steric repulsions, possibly through the adduct-like coordination of the $\mu_2$-FeCp′(CO) groups to the electron pairs on P7 and P8.

Since one can visualize the formation of $\alpha$-$P_8$ via a coalescence of photolytically generated $P_2$ units, it follows that the realgar-type structure of $\alpha$-$P_8$ is most probably the kinetically favored configuration compared to the thermodynamically favored homonorborane configuration of $\beta$-$P_8$ (Figure 6). Chelating $P_2$ units in $P_n$ structures and the $\mu_2$-Fe bridges in **1** and **2** trap this thermodynamically disfavored $\alpha$-$P_8$ unit, preventing it from isomerizing. A further investigation into the potential stabilizing effects of electron-withdrawing inorganic or organometallic substituents on polyphosphide clusters is merited.

**Acknowledgment.** The authors thank the National Science Foundation for its support of this research. Additionally, we are indebted to Ken Rouse (UW—Madison) for literature-search assistance and to Professor Brock Spencer (Beloit College) and Professor June Dahl (UW—Madison) for helpful advice.

**Supplementary Material Available:** Tables listing assigned major ion peaks with relative abundances for positive- and negative-ion LD/FT mass spectra of $Cp'_4Fe_4(CO)_6P_8$ (**1**) and $Cp'_4Fe_6(CO)_{13}P_8$ (**2**), coordinates and anisotropic thermal parameters for the non-hydrogen atoms, and fixed positional isotropic thermal parameters for the hydrogen atoms for **1** and **2** (10 pages); tables of observed and calculated structure factor amplitudes for **1** and **2** (47 pages). Ordering information is given on any current masthead page.